J Mater Sci: Mater Med (2010) 21:2355–2364
DOI 10.1007/s10856-010-4089-2

A spectroscopic investigation into the setting and mechanical properties of titanium containing glass polyalkenoate cements

A. W. Wren · A. Kidari · N. M. Cummins · M. R. Towler

Received: 5 March 2010 / Accepted: 26 April 2010 / Published online: 13 May 2010

Abstract Titanium (Ti) implants are extensively used in a number of biomedical and dental applications. This work introduces Ti into the glass phase of a zinc based glass polyalkenoate cement (GPC) and investigates changes in handling and mechanical properties considering two molecular weight polyacrylic acids (PAA), E9 and E11. Considering the handling properties, the working time (T_w) increased from 50 s_{E9}, 32 s_{E11} (BT 101, Ti-free) to 169 s_{E9}, 74 s_{E11} with TW-Z (highest Ti content), respectively. The setting time (T_s) increased from 76 s_{E9}, 47 s_{E11} (BT 101) to 303 s_{E9}, 232 s_{E11} with TW-Z, respectively. Ti was also found to have a significant increase on both compressive (σ_c) and biaxial flexural strength (σ_f), where σ_c increased from 36 MPa_{E9}, 56 MPa_{E11} (BT 101) to 56 MPa_{E9} and 70 MPa_{E11} with TW-Z respectfully. σ_f also increased from 11 MPa_{E9}, 22 MPa_{E11} (BT 101) to 22 MPa_{E9} and 77 MPa_{E11} with TW-Z, respectively. No increase in mechanical properties was evident with respect to maturation. Raman Spectroscopy was employed to investigate changes in glass structure and the setting of the cements with. This revealed increased glass network disruption with increasing TiO_2 content and matured cement setting with TW-Z as compared to the control BT 101. FT-IR was then employed to investigate any additional setting mechanism and changes with time. Spectroscopy determined that Ca^{2+}/Sr^{2+}PAA complexes are primarily responsible for the setting and mechanical strength with no changes occurring over time.

A. W. Wren (✉) · M. R. Towler
Inamori School of Engineering, Alfred University, Alfred, NY 14802, USA
e-mail: wren@alfred.edu

A. Kidari · N. M. Cummins
Materials and Surface Science Institute, University of Limerick, Limerick, Ireland

1 Introduction

The use of titanium (Ti) and its alloys in the field of biomaterials has increased recently due to a number of desirable properties. It has been used for fabrication of bone-anchored metal implants in orthopedic reconstruction, oral-maxillofacial [1], dentistry (crowns, bridges and partial dentures) [2] and as ossicular implants [3, 4] due to a number of attributes including high mechanical strength, corrosion resistance and excellent biocompatibility compared to other base metals [5, 6]. The biocompatibility of Ti is attributed to the formation of an oxide layer in contact with biological tissues [6]. This protective layer in bone can grow in thickness and facilitate ion exchange, however, the low rate of dissolution and the chemical inertness of Ti dissolution products allow bone to thrive and osteointegrate with Ti [7]. Studies by Takadama et al. [8] has found that Ti can be highly bioactive by being soaked in NaOH and heat treated. This resulted in the bonding and integration of Ti with living bone by the formation of a bonelike apatite layer on its surface. This interaction is induced by functional groups such as Ti–OH which introduces a negative surface charge thus inducing apatite formation [9]. The described properties suggest that Ti based implants are beneficial in both medical and dental procedures such as hip arthroplasty and as dental roots [8].

This work sees the addition of Ti to the glass phase of a Ca–Sr–Zn–Si based glass polyalkenoate cement (GPC) with the intended application being vertebral stabilization/restoration. Ti was added initially due to its excellent biocompatibility, however it has also been described as

having a structural role in a glass as a network intermediate, where it can act as either a network former or modifier [10]. Preliminary studies on these Ti-based glasses included up to 0.20 mol% addition of Ti, however it was found that by increasing the concentration of Ti, the ratio of Non-Bridging Oxygen to Bridging Oxygen (NBO:BO) increased resulting in a highly disrupted glass network. This indicates that Ti has predominantly a network modifying role. For this work a series in the region of 0.05 mol% Ti was added as stable cements can be formed [11].

Previous work on the Ca–Sr–Zn–Si GPCs has demonstrated the handling and mechanical properties of these cements [12]. This initial formulation was chosen as both zinc (Zn) and strontium (Sr) are known to have a number of benefits in vivo. Both Zn and Sr are known to have bone metabolic abilities [13–16] while Zn is also known to be antibacterial in nature [17–19] and Sr will impart radiopacity to the material. The silica (Si) and calcium (Ca) in the glass perform a structural role while also imparting bioactivity while in the form of a cement. However one of the major drawbacks to the use of this cement is the restricted handling properties [12] as compared to some of the commercial GPCs [20] or PMMA [20–22] based bone cements. The handling properties, in this case the working time (T_w) and the setting time (T_s), are considered important characteristics in considering cements for implantation. Cements with extended T_s can lead to septic complications which can lead to revision surgeries and considerable suffering to the patient [23], and cements that set too quickly can compromise the cement structure, thereby reducing the mechanical strength. It has previously been discussed in the literature that the optimal T_s for a bone cement is in the region of 5–8 min [24].

This work sees the addition of Ti to this Ca–Sr–Zn–Si GPC in order to determine if any specific changes in handling or mechanical strength occurs. Raman Spectroscopy and FT-IR were also employed to investigate any structural changes in the glass, the set cement comparative to polyacrylic acid (PAA) and also any changes occurring over time.

2 Materials and methods

2.1 Glass synthesis

Four glass compositions were formulated for this study with the principal aim being to investigate the substitution of Si with Ti throughout the glass series. BT 101 was used as a control and cements denoted TW-X, TW-Y and TW-Z contain incremental concentrations of Ti at the expense of Silica (Si). Glasses were prepared by weighing out appropriate amounts of analytical grade reagents (Sigma–Aldrich, Dublin, Ireland) and ball milling (1 h). The mix was then oven dried (100°C, 1 h) and fired (1,500°C, 1 h) in a platinum crucible and shock quenched into water. The resulting frit was dried, ground and sieved to retrieve a glass powder with a maximum particle size of 45 μm (Table 1).

Table 1 Glass composition used in this study

	BT 101	TW-X	TW-Y	TW-Z
SiO_2	0.480	0.464	0.448	0.430
TiO_2	0.000	0.016	0.032	0.050
ZnO	0.360	0.360	0.036	0.036
CaO	0.120	0.120	0.012	0.012
SrO	0.040	0.040	0.040	0.040

2.2 Glass characterisation

2.2.1 Network connectivity (NC)

The NC of the glasses was calculated with Eq. 1 using the molar compositions of the glass. NC calculations were performed assuming that Ti performs as a network former and also as a network modifier.

$$\mathrm{NC} = \frac{\text{No. BOs} - \text{No. NBOs}}{\text{Total no. bridging species}} \quad (1)$$

where NC, network connectivity; BO, Bridging Oxygens; and NBO, Non-Bridging Oxygens.

2.2.2 Differential thermal analysis (DTA)

A combined differential thermal analyser-thermal gravimetric analyser (DTA-TGA) (Stanton Redcroft STA 1640, Rheometric Scientific, Epsom, UK) was used to measure the glass transition temperature (T_g) for both glasses. A heating rate of 10°C min^{-1} was employed using an air atmosphere with alumina in a matched platinum crucible as a reference. Sample measurements were carried out every 6 s between 30 and 1,000°C.

2.2.3 X-ray diffraction (XRD)

Diffraction patterns were collected using a Philips Xpert MPD Pro 3040/60 X-ray Diffraction Unit (Philips, Netherlands). Disc samples (32 mm ∅ × 3 mm) were prepared by pressing a selected glass powder (<45 μm) into a backing of ethyl cellulose (8 tonnes, 30 s). Samples were then placed on spring-back stainless steel holders with a 10 mm mask and were analysed using Cu K_α radiation. A generator voltage of 40 kV and a tube current of 35 mA was employed. Diffractograms were collected in the range

$5° < 2\theta < 80°$, at a scan step size 0.0083° and a step time of 10 s. Any crystalline phases present were identified using JCPDS (Joint Committee for Powder Diffraction Studies) standard diffraction patterns.

2.3 Cement preparation

Cements were prepared by thoroughly mixing the glass powders (<45 μm) with E9 and E11 polyacrylic acid (PAA—M_w, 80,800 and 210,000, <90 μm, Advanced Healthcare Limited, Kent, UK) and distilled water on a glass plate. The cements were formulated in a P:L ratio of 2:1.5 with 50 wt% additions of PAA, where 1 g of glass powder was mixed with 0.37 g E9 PAA and 0.37 ml water. Complete mixing was undertaken within 20 s.

2.4 Working and setting times

The setting times (T_s) of the cement series were tested in accordance with ISO9917 which specifies the standard for dental water based cements [25]. The working time (T_w) of the cements was measured in ambient air using a stop-watch, and was defined as the period of time from the start of mixing during which it was possible to manipulate the material without having an adverse effect on its properties.

2.5 Mechanical properties

2.5.1 Compressive strength

The compressive strengths (σ_c) of the cements were evaluated in accordance with ISO9917 [25]. Cylindrical Samples were tested after 1, 7 and 30 days. Testing was undertaken on an Instron 4082 Universal Testing Machine (Instron Ltd., High Wycombe, Bucks, UK) using a 5 kN load cell at a crosshead speed of 1 mm/min^{-1}.

2.5.2 Biaxial flexural strength

The flexural strengths (σ_f) of the cements were evaluated by a method described by Williams et al. [26]. Cement discs were tested after 1, 7 and 30 days. Testing was undertaken on an Instron 4082 Universal Testing Machine (Instron Ltd., High Wycombe, Bucks, UK) using a 1 kN load cell at a crosshead speed of 1 mm/min^{-1}.

2.6 Sample preparation for spectroscopy

For Raman Spectroscopy, both glass frit (Sect. 2.1) and cement powder were used while cement powder only was required for FT-IR. Initially cement discs prepared as described in Sect. 2.7, were immersed in de-ionised water for 24 h to remove any excess PAA. The cement discs were then dried in an oven at 37°C for 1 h and ground to a <45 μm powder. The cement powder was then desiccated for 6 h to remove any excess water.

2.7 Raman spectroscopy

Raman spectra were collected on glass frit/cement powder samples using a DILOR XY Labram (Horiba Jobin–Yvon Inc., NJ, USA) with a He–Ne 20 mW laser (green source at 514.5 nm) under a tension of 7.45 mA. A grating number of 1,800 was used in association with a Peltier cooled CCD detector and the system was coupled to a confocal microscope Olympus model BX40.

2.8 Fourier transform infrared spectroscopy (FT-IR)

FT-IR spectra were obtained by the KBr disc method using a Perkin Elmer Spectrum 100 Series spectrometer (Perkin Elmer, Dublin, Ireland). Analysis was performed in the mid-infrared region (4,000–400 cm^{-1}) with a spectral resolution of 4 cm^{-1}.

2.9 Statistical analysis

One-way analysis of variance (ANOVA) was employed to compare the handling and mechanical properties of the Ti cements to the control BT 101 cement and where relevant, any changes occurring with respect to maturation. Comparison of relevant means was performed using the post hoc Bonferroni test. Differences between groups was deemed significant when $P \leq 0.05$. Statistical analysis was performed using SPSS software for windows version 16 (SPSS Inc. Chicago, IL).

3 Results and discussion

The primary objective of this study was to incorporate Ti into a Ca–Sr–Zn–Si GPC. This was accomplished due to the numerous publications citing the biocompatibility of Ti in the body. Previous work on the glass phase of this series found that additions in excess of 0.20 mol% TiO_2 resulted in crystallinity, and glasses with TiO_2 content between 0.05 and 0.20 mol% did not form cements due to the highly disrupted network [11]. Characterization of the glass phase of this cement series was carried out using XRD, DTA and NC calculations. Results of the characterization can be seen in Fig. 1.

From Fig. 1a it can be seen from XRD that no crystallinity is present in any of the glasses used to make the cements. The NC of the glass series (Fig. 1b) was seen to decrease from 1.83 (BT101) to 1.35 (TW-Z) as the TiO_2 content in the glass increased. This suggests that the

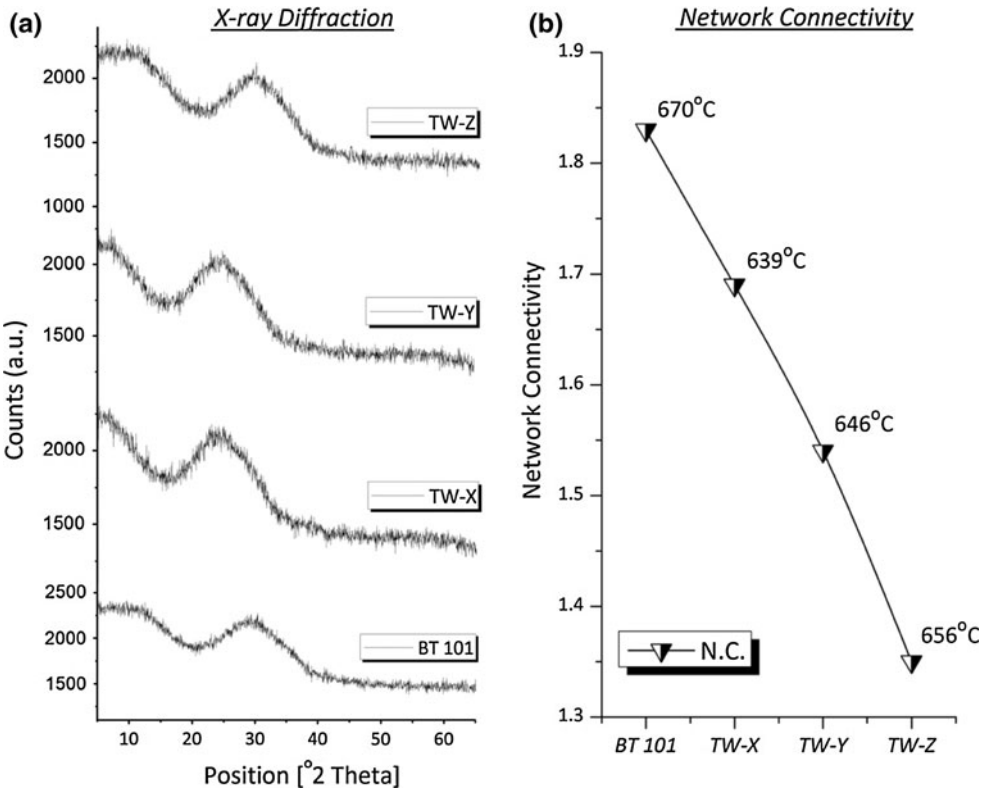

Fig. 1 Characterization of glass series **a** XRD and **b** NC and T_g

addition of TiO_2 increases the level of disruption within the glass network, causing the formation of Si–NBO bridges. This agrees with previous work on similar glasses [11]. The T_g of the glass, as determined by DTA (Fig. 1b), was found to decrease initially from 670°C (BT 101) to 639°C (TW-X) with the addition of 0.016 mol% TiO_2. However, the T_g increased from 639°C (TW-X) to 656°C (TW-Z) with additions of up to 0.05 mol% TiO_2. From Fig. 1b it can be determined that the addition of TiO_2 increases the level of network disruption, however the slight increase in T_g may suggest another structural role for Ti at this level, however this increase may also be due to natural variation and be insignificant.

Determination of the handling properties was the next stage where the working time (T_w) and setting time (T_s) were evaluated for each of the cements. Each of the cements, (BT 101, TW-X, TW-Y and TW-Z) were mixed with E9 and E11 PAA, as the PAA molecular weight will have a significant effect on both the handling properties and the resulting mechanical properties. Figure 2a presents the T_w of the cement series while Fig. 2b shows the T_s.

In relation to the T_w, TW-X (53 s) tested with E9 showed no significant change when compared to the control cement, BT 101 (50 s). However, TW-Y (77 s, $P \leq 0.0001$) and TW-Z (168 s, $P \leq 0.0001$) showed a significant increase when compared to BT 101. A similar trend occurred in relation to the E11 cements where no significant change occurred between BT 101 (32 s) and TW-X (32 s), however significant increases did occur with TW-Y (48 s, $P \leq 0.0001$) and TW-Z (74 s, $P \leq 0.0001$).

T_s were also found to significantly increase at each time point with the increase in TiO_2 content. Regarding E9 PAA (Fig. 2b), cements increased from 76 s (BT101) to 133 s (TW-X, $P \leq 0.0001$), to 157 s (TW-Y, $P \leq 0.0001$) to 302 s (TW-Z, $P \leq 0.0001$), where TW-Z E9 PAA achieved the longest T_s of any of the cements. In relation to E11 PAA, a similar trend was observed where the T_s increased from 47 s (BT101) to 86 s (TW-X, $P \leq 0.0001$), to 123 s (TW-Y, $P \leq 0.0001$) to 232 s (TW-Z, $P \leq 0.0001$). The increase in the T_w and T_s in this case is as a result of increasing TiO_2 concentration, which in the case of E11 PAA facilitates the use of this acid. Also the addition of 0.05 mol% TiO_2 to TW-Z E9 PAA, increased the T_s to the desired T_s for vertebroplastic bone cements as suggested by Heini et al. [24].

The compressive strengths (σ_c) of each of the cements was statistically tested with respect to maturation and also compared to the control cement, BT 101. Figure 3 shows the σ_c of cements formulated with both E9 and E11 PAA.

In relation to maturation and cements produced with E9 PAA (Fig. 3a), BT 101 increased in strength significantly between 1 and 7 day (36–41 MPa, $P \leq 0.044$), however 7–30 day (41–45 MPa) did not reach significance. Regarding the Ti cements there was no significant changes over time with the exception of TW-Y, 1–30 day, $P \leq 0.001$. In comparing the Ti series to the control cement BT

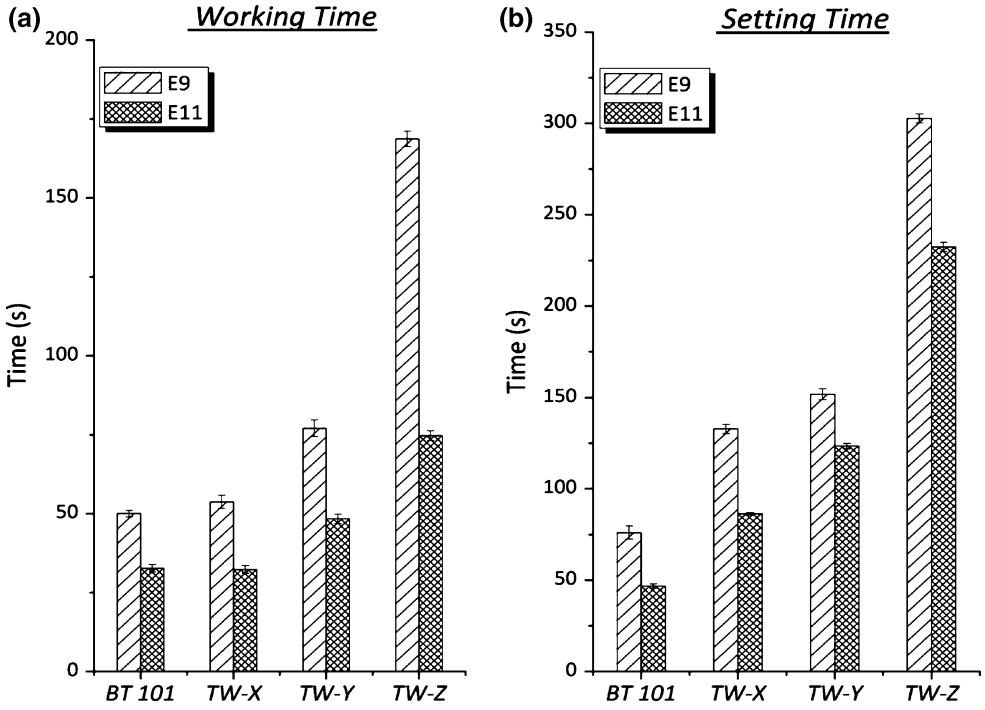

Fig. 2 Working and setting times of Ti—cement series

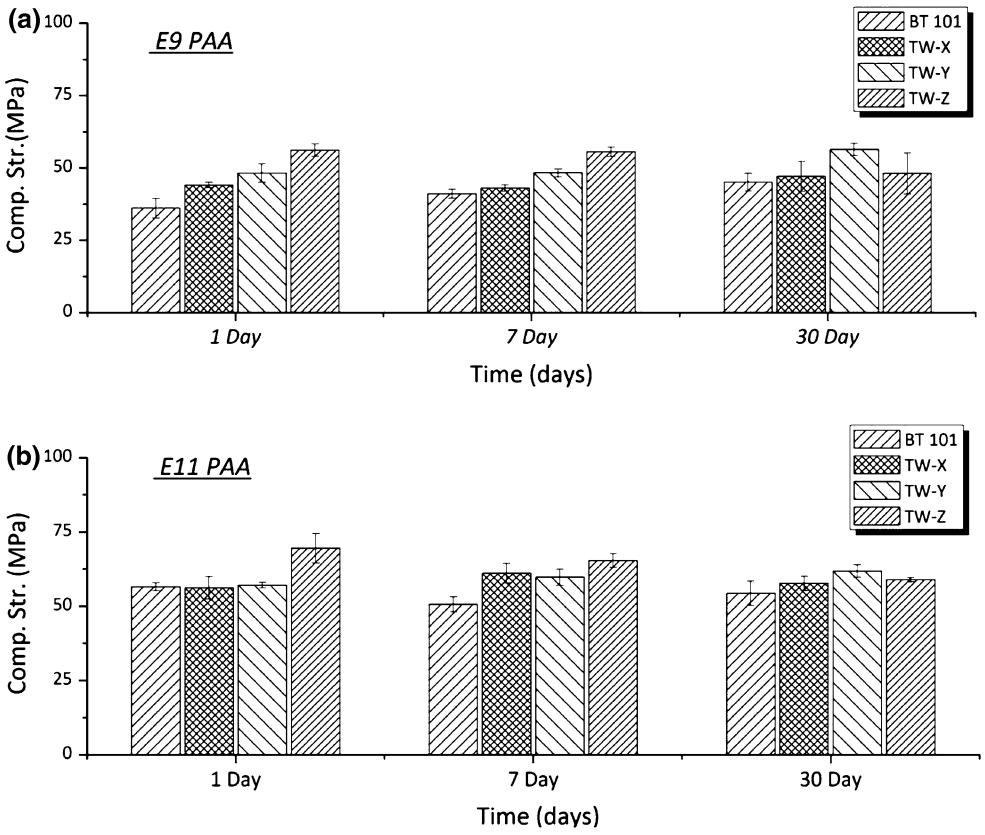

Fig. 3 Compressive strength of **a** E9 and **b** E11 cement series

101, significant increases in strength were observed. At 1 day, TW-X (44 MPa, $P \leq 0.004$), TW-Y (48 MPa, $P \leq 0.000$) and TW-Z (56 MPa, $P \leq 0.0001$) increased significantly in strength when compared to BT 101. At 7 day significant increases in strength were observed with TW-Y (48 MPa, $P \leq 0.0001$) and TW-Z (55 MPa,

$P \leq 0.0001$), while at 30 day significance was only reached with TW-Y (56 MPa, $P \leq 0.024$).

Regarding E11 PAA (Fig. 3b), the σ_c of the cements exhibited little change with respect to maturation. BT 101 reduced in strength between 1 and 7 days (56–51 MPa, $P \leq 0.020$) while there was no significant change with TW-X over 1–30 days (56–58 MPa). Both TW-Y and TW-Z only showed significant change when comparing 1–30 days, 57–61 MPa, ($P \leq 0.009$), and 70–59 MPa, ($P \leq 0.001$), respectively. In comparing the Ti cements to the control BT 101 (51 MPa), significant increases were found at 1 day with TW-Z (70 MPa, $P \leq 0.0001$). At 7 days, a significant increase in σ_c was found with each of the Ti cements, TW-X (61 MPa, $P \leq 0.0001$), TW-Y (60 MPa, $P \leq 0.0001$) and TW-Z (65 MPa, $P \leq 0.0001$). At 30 days, significance was only achieved between BT 101 and TW-Y (54–62 MPa, $P \leq 0.002$). It can be seen from the σ_c that the addition of TiO_2 is having an effect on cement strength when compared to the control; however it can also be observed that little change is occurring with respect to time. In comparing the σ_c of commercial materials of similar chemistry, GPCs such as Fuji IX have a σ_c of 211 MPa [20]. The σ_c of the experimental cements under evaluation here are considerably lower. This may be attributed primarily to the structure of the glass used. Commercial GPCs contains aluminum (Al^{3+}) which provides an important structural role where it depolymerizes the silicate network facilitating acid degradability, while also forming Al–PAA complexes during setting, which results in higher mechanical strength [27]. Additives such a tartaric acid can slow the setting rate [28], which possibly also contributes to matured setting and increased mechanical strength.

In relation to the σ_f produced with E9 PAA (Fig. 4a), there was no significant change in strength for any of the cements with respect to maturation, the highest being TW-Y at 7 days, 22 MPa. However, changes did occur when comparing the Ti cements to the control, BT 101 (11 MPa). At 1 day, significance was reached with TW-X (15 MPa, $P \leq 0.0001$), TW-Y (19 MPa, $P \leq 0.0001$) and TW-Z (19 MPa, $P \leq 0.0001$). A similar trend was observed at 7 days where changes occurred between the Ti cements and BT 101, TW-X (18 MPa, $P \leq 0.0001$), TW-Y (22 MPa, $P \leq 0.0001$) and TW-Z (18 MPa, $P \leq 0.0001$). At 30 days, significance was only reached by TW-Y (21 MPa, $P \leq 0.038$). Considering cements formulated with E11 PAA (Fig. 4b), no significant changes occurred with respect to time with any of the cements, however, similarly to the σ_c, overall strengths were increased by using E11 PAA with a maximum of 77 MPa with TW-Z. When comparing the Ti cements to the control BT 101 (39 MPa), a significant increase was evident with each cement at 1 day where TW-X (51 MPa, $P \leq 0.032$), TW-Y (64 MPa, $P \leq 0.0001$) and TW-Z (66 MPa, $P \leq 0.0001$). At 7 and 30 days, changes were only evident with TW-Z, 76 MPa, ($P \leq 0.013$) and 72 MPa ($P \leq 0.028$). It can be determined from the mechanical testing that there was a general trend for the mechanical properties to increase with increasing TiO_2 content when compared to the control, Ti-free BT 101. However, in each case there was little change in strength with respect to maturation.

In order to determine how the handling (T_w and T_s) and mechanical properties (σ_c and σ_f) increased with TiO_2 addition, Raman and FT-IR Spectroscopy were employed. Raman Spectroscopy was initially used to determine changes in the glass structure that will subsequently affect the setting and mechanical strength. Secondly, it was used to determine any changes in the set cement comparative to PAA. Figure 5 shows the Raman spectra for the control glass BT 101 and the glasses used to make the Ti cements.

Raman spectra for BT 101 agrees with NC calculations where predominantly Q^1/Q^2 structures are present, identified by the main peak occurring at 980 cm^{-1} with a shoulder appearing at 880 cm^{-1} which relate to the symmetrical stretching motion of Si–NBO bonds in Q^2 and Q^1 tetrahedra, respectively. Since the main band envelope extends up to 1,100 cm^{-1}, Q^3 units may also be present as they lie around 1,100 cm^{-1} and a minor fraction of Q^0 species can be also be considered as suggests the low wavenumber region of the same band [29]. It is evident that as the TiO_2 concentration in these glasses increases, there is an overall shift of the Raman spectra to lower wavenumbers in addition to a decrease in the count rate recorded within the regions associated with Q^1 and Q^2 silicate units. This decrease becomes significant only for glasses TW-X and TW-Y, however it is less obvious for glass TW-X which comprises the lowest Ti substitution rate in this series. This is also reflected by the changes occurring between BT101 and TW-X in T_w, σ_c and σ_f which were found to be less significant than for the remaining glasses.

For TW-X (0.016 TiO_2) the highest intensity is recorded at the same position as in the Ti-free glass BT101, then, it shifts down to 944 cm^{-1} for TW-Y (0.032 TiO_2) where a prominent peak can be found at 870 cm^{-1} along with a wide shoulder of low intensity extending from 806 down to 620 cm^{-1}. In the Ti–rich end of this series (TW-Z with 0.050 TiO_2), the most intense features can be found at 867 and 780 cm^{-1}. The changes occurring in the low wavenumber region are attributed to the presence of six-fold coordinated titanium cations which are reported at 780 cm^{-1} [30, 31] and subsequently the continuous shift to lower wavenumbers results from the depolymerization of the silicate network. The fraction of Q^1 and Q^0 species increases at the expense of Q^2 silicate units as indicates the rising intensity around 900 and 850 cm^{-1} for Q^1 and Q^0 units, respectively [29]. The main peak present in TW-Z at

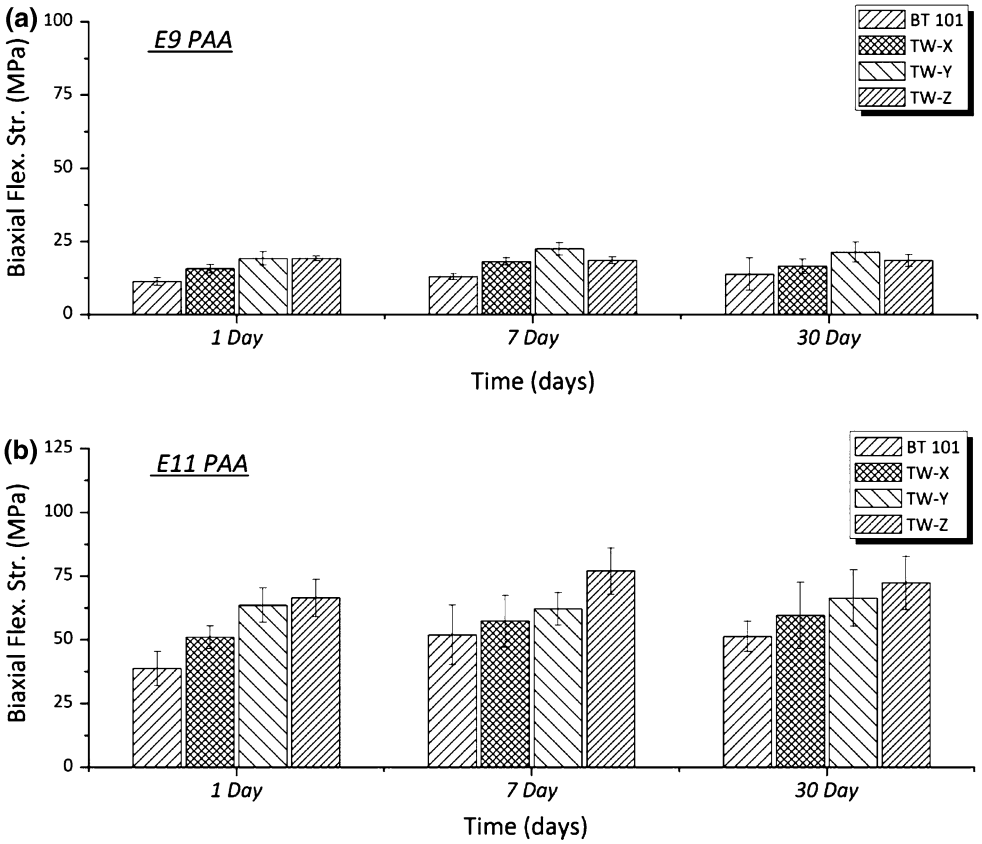

Fig. 4 Biaxial flexural strength of **a** E9 and **b** E11 cement series

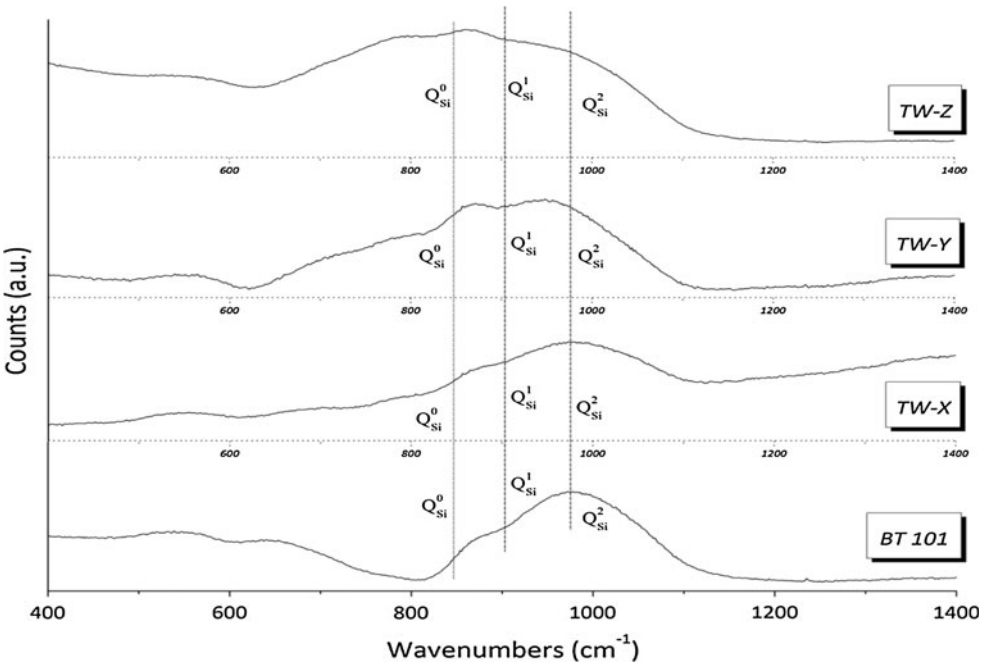

Fig. 5 Raman spectra of BT 101, TW-X, TW-Y and TW-Z glass

867 cm^{-1} indicates a complete shift from Q^1/Q^2 (BT101) to predominantly Q^1/Q^0 (TW-Z) silicate structures. The addition of TiO_2 therefore results in depolymerization of the silicate network, which will result in greater cationic activity during the setting reaction particularly with TW-Z compared to BT 101.

Further Raman studies were conducted on the set cements to determine how these ions interact with PAA

when set. Figure 6 shows the Raman spectra of E11 PAA, BT 101 and TW-Z cements.

It is well known that the setting of GPCs is related to cations from the glass, (Ca^{2+}, Sr^{2+}, Al^{3+}, Zn^{2+}), depolymerising the silicate network [32] and subsequently forming ionic crossbridges with COO^{-} groups from the PAA chain [33–35]. Figure 6a shows the Raman Spectra of E11 PAA and its associated peaks. Previous studies by Dong et al. [36] has identified the major peaks associated with PAA and are listed in Table 2. As did Young et al. [37] in their study of GPC setting which in addition, also determined the salts of Na–PAA, Ca–PAA and Al–PAA. The Raman spectra for PAA (Fig. 6a) contains relatively broad peaks which are typical of these polymers; the PAA spectrum in this study closely resembles PAA spectra from previous work (Table 2) [36, 37].

It is initially evident that upon neutralization the peak at 1,674 cm^{-1} (C=O) in the spectrum of pure PAA is absent from both BT 101 and TW-Z. Peaks found at 1,588 cm^{-1} (weak for COO) and at 1,457 cm^{-1} (strong for CH_2) in the spectrum of the TW-Z glass agree well with the literature [37] for Ca–PAA salts (Table 2), meanwhile the intensity of the CH_2 peak was found to be lower in BT 101 while the 1,588 cm^{-1} peak for COO could not be extracted. Peaks present around 1,460, 1,300 and 1,100 cm^{-1} are primarily due to the polymer backbone, and these are clearly evident in the Raman spectrum of the reacted TW-Z glass at 1,457, 1,329 and 1,102 cm^{-1}. This is in agreement with previous studies which state that these peaks remain clearly identifiable upon neutralization and therefore demonstrates that glass particles dissolution occurred on a larger scale for this glass [37].

Table 2 Raman assignment for PAA and Ca–PAA

PAA [36, 37]	BT 101	TW-Z	Ca–PAA [37]	Ref. [36, 37]
1,674				
		1,588	1,588	Assym. COO
1,452		1,457	1,457	CH_2 Def.
	1,401			
		1,424	1,427	Sym COO
1,330		1,329	1,329	CH_2 Twist
1,102	1,102	1,102	1,096	C–CH_2 Stretch
	914	916	913	C–COO Stretch
	876	878	865	C–COO Stretch

Raman Spectroscopy of the non-reacted glasses showed that increasing TiO_2 content de-polymerizes the silicate glass network resulting in a higher concentration of Si–NBO bonds which enhance the acid degradability of the glass. In the set cement it can be seen that Ca plays the primary role in forming crosslinks during setting, and that the degree of crosslinking in BT 101 is limited. However, the information available on Raman spectroscopy applied to GPC are limited to Ca–PAA so that the occurrence of Sr–PAA cannot be confirmed unequivocally. Meanwhile, similarities in the structural role taken by these cations and their close atomic characteristics avail the idea that Sr–PAA could occur in the cement structure along with Ca–PAA [38].

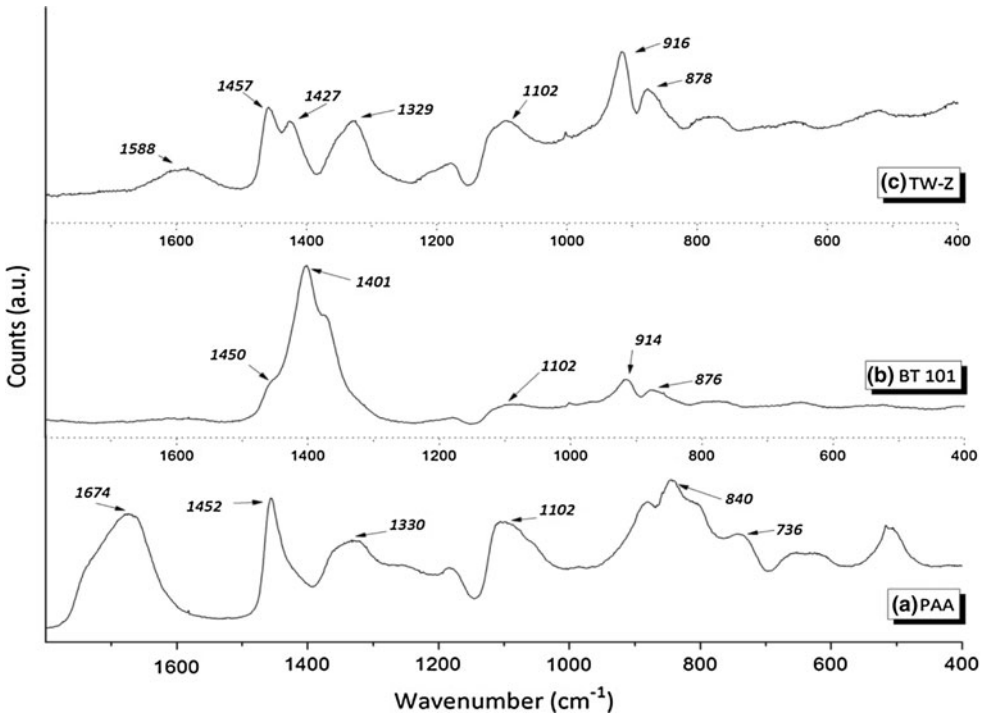

Fig. 6 Raman spectra of (*a*) PAA, (*b*) BT 101 and (*c*) TW-Z cement powder

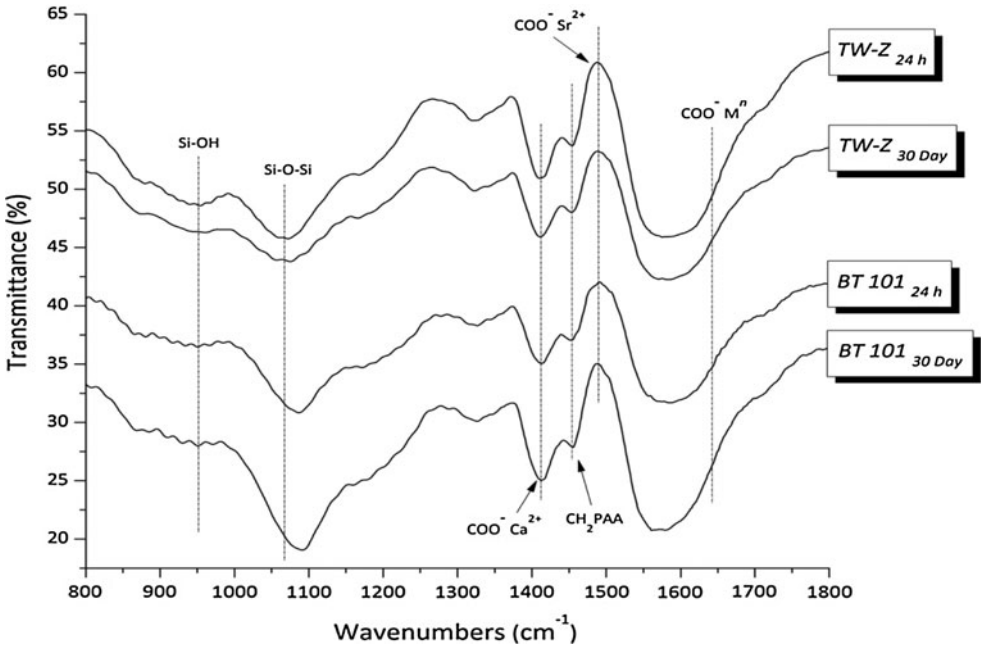

Fig. 7 FT-IR spectra of BT 101 and TW-Z cements

Further studies were performed by FT-IR in order to identify any additional bonding mechanisms and also to determine if any changes in the cements structure occurs with respect to maturation. Figure 7 shows a comparison of 1 and 30 days for both BT 101 and TW-Z cements.

In relation to the cements under investigation here, $COO^{-}Ca^{2+}$ and $COO^{-}Sr^{2+}$ bridges were identified at 1,415 cm^{-1} [35] and within the range 1,460–1,490 cm^{-1} [35], respectively, which agrees with previous work by Tomlinson et al. [35]. Also in the region of 1,540–1,630 cm^{-1}, both $COO^{-}Ca^{2+}$ and $COO^{-}Sr^{2+}$ groups are formed. In this instance the symmetry of the band suggest a fully set cement when compared to $COO^{-}M^{n+}$ ($n = Al^{3+}$, Ca^{2+}, Sr^{2+}) forming complexes in commercial GPCs [39], indicating that in this case both Ca^{2+} and Sr^{2+} are the prominent crosslinking ions during the setting reaction. Previous studies by Nicholson et al. [28] reported Ca–PAA complexes in the region of 1,550 cm^{-1} when studying the effect of (+)-tartaric acid on GPCs, and earlier studies by Crisp et al. [40] also found Ca–PAA complexes in the region of 1,560 cm^{-1}. It is also evident that there is no shift in wavenumber over time suggesting that the cements have a final set within 24 h, which agrees with mechanical properties. Also little change was seen with the addition of TiO_2, however, a slight variation was observed in the region 1,000–1,100 cm^{-1} which is attributed to differences in Si–O–Si and Si–NBO groups and the formation of Si–OH vibration modes [34, 35, 39]. FT-IR was able, in this case, to distinguish the primary salt forming ions, and that little changes were occurring with respect to time.

It is likely in these cements that Ti is slowing the acid–base setting reaction by either adjusting the pH at setting or by reducing the availability of Zn within the glass. It likely does this by charge compensation with Zn, as Ti requires neutralization when in an electrically unstable environment. The reduced Zn content facilitates longer T_w and T_s and promotes increased mechanical strength by permitting the formation of matured Ca (and Sr)–PAA complexes. Regarding this study, Raman Spectroscopy determined that a higher degree of particle dissolution and ion integration occurs as the Ti concentration increases in the glass series, and also that crosslinking within the set cement occurs by the formation of Ca–PAA complexes. FT-IR supports this, with the additional identification of Sr–PAA complexes, and also that the maturation of these cements is completed within 24 h which is reflected in the mechanical properties.

Acknowledgements Enterprise Ireland Grant, TD/2005/327.

References

1. Byon E, Moon S, Cho S-B, Jeong C-Y, Jeong Y, Sul Y-T. Electrochemical property and apatite formation of metal ion implanted titanium for medical implants. Surf Coat Technol. 2005;200(1–4):1018–21.
2. González JEG, Mirza-Rosca JC. Study of the corrosion behavior of titanium and some of its alloys for biomedical and dental implant applications. J Electroanal Chem. 1999;471(2):109–15.
3. Schwager K. Titanium as a biomaterial for ossicular replacement: results after implantation in the middle ear of the rabbit. Eur Arch Otorhinolaryngol. 1998;255:396–401.
4. Lausmaa J. Surface Spectroscopic characterization of titanium implant materials. J Electron Spectrosc Relat Phenom. 1996;81:343–61.
5. Fawzy AS, El-Askary FS. Effect acidic and alkaline/heat treatments on the bond strength of different luting cements to commercially pure titanium. J Dent. 2009;37:255–63.

6. Turpin YL, Tardive RD, Tallec A, Le Menn AC. Corrosion susceptibility of titanium covered by dental cements. Dent Mater. 2000;16:57–61.
7. Takeuchi M, Abe Y, Yoshida Y, Nakayama Y, Okazaki M, Akagawa Y. Acid pretreatment of titanium implants. Biomaterials. 2003;24(10):1821–7.
8. Takadama H, Kim H-M, Kokubo T, Nakamura T. XPS study of the process of apatite formation on bioactive Ti-6Al-4V alloy in simulated body fluid. Sci Technol Adv Mater. 2001;2:389–96.
9. Kokubo T, Kim H-M, Kawashita M. Novel bioactive materials with different mechanical properties. Biomaterials. 2003;24: 2161–75.
10. Nicholson JW, Wilson AD. Acid-base cements—their biomedical and industrial applications. In: West AR, Baxter H, editors. Chemistry of solid state materials. Vol. 3. Cambridge: Cambridge University Press; 1993.
11. Wren AW, Laffir FR, Kidari A, Towler MR. The Structural Role of Titanium in Ca–Sr–Zn–Si/Ti Glasses for Medical Applications. J Non-Cryst Solids. 2010 (Submitted manuscript).
12. Wren AW, Boyd D, Towler MR. The processing, mechanical properties and bioactivity of strontium based glass polyalkenoate cements. J Mater Sci: Mater Med. 2008;19:1737–43.
13. Marie PJ. Strontium ranelate; a novel mode of action optimizing bone formation and resorption. Osteoporos Int. 2005;16:S7–10.
14. Marie PJ. Strontium ranelate: new insights into its dual mode of action. Bone. 2007;40(5):S5–8.
15. Yamaguchi M, Ma ZJ. Role of endogenous zinc in the enhancement of bone protein synthesis associated with bone growth of newborn rats. J Bone Miner Metab. 2001;19:38–44.
16. Yamaguchi M, Ma ZJ. Stimulatory effect of zinc on Deoxyribonucleic acid synthesis in bone growth of newborn rats:enhancement with zinc and insulin like growth factor-I. Calcif Tissue Int. 2001;69:158–63.
17. Wren AW, Boyd D, Thornton R, Cooney JC, Towler MR. Antibacterial properties of a tri-sodium citrate modified glass polyalkenoate cement. J Biomed Mater Res B. 2009;90-B(2): 700–9.
18. Sawai J. Quantative evaluation of antibacterial activities of metallic oxide powders (ZnO, MgO and CaO) by conductimetric assay. J Microbiol Methods. 2003;54:177–82.
19. Yamamoto O. Influence of particle size on the antibacterial activity of zinc oxide. Int J Inorg Mater. 2001;3:643–6.
20. Higgs WA, Lucksanasombool P, Higgs RJED, Swain MV. Comparison of the material properties of PMMA and glass ionomer based cements for use in orthopaedic surgery. J Mater Sci: Mater Med. 2001;12:453–60.
21. Khun K-D. Bone cements: up-to-date comparison of physical and chemical properties of commercial materials. New York: Springer; 2000.
22. Dunne NJ, Orr JF. Thermal characteristics of curing acrylic bone cement. ITBM-RBM. 2001;22(2):88–97.
23. Bahna P, Dvorak T, Hanna H, Yasko AW, Hachem R, Raad I. Orthopaedic metal devices coated with a novel antiseptic dye for the prevention of bacterial infection. Int J Antimicrob Agents. 2007;29:593–6.
24. Heini P, Berlemann U. Bone substitutes in vetebroplasty. Eur Spine J. 2001;10:S205–13.
25. International Organization for Standardization 9917. Dental Water Based Cements (E), in Case Postale 56: Geneva, Switzerland, CH-11211; 1991.
26. Williams JA, Billington RW, Pearson GJ. The effect of the disc support system on biaxial tensile strength of a glass ionomer cement. Dent Mater. 2002;18:376–9.
27. Nicholson JW. Chemistry of glass ionomer cements. Biomaterials. 1998;19:485–94.
28. Nicholson JW, Brookman PJ, Lacy OM, Wilson AD. Fourier transform infrared spectroscopic study of the role of tartaric acid in glass ionomer cements. J Dent Res. 1988;67:1451–1454.
29. McMillian PW. Structural studies of silicate glasses and melt-applications and limitations of Raman spectroscopy. Am Mineral. 1984;69:622–44.
30. Iwamoto N, Tsunawaki Y, Masao F, Hatfori T. Raman spectra of K_2O-SiO_2 and K_2O-SiO_2-TiO_2 glasses. J Non-Cryst Solids. 1975; 18:303–6.
31. Kusaeiraki K. Infrared and Raman spectra of vitreous silica and sodium silicates containing titanium. J Non-Cryst Solids. 1987;95 & 96:411–8.
32. Chen CC, Ho C-C, Chen C-HD, Ding S-J. Physicochemical properties of calcium silicate cements for endodontic treatment. J Endod. 2009;35(9):1288–91.
33. Xie D, Feng D, Chung I, Eberhardt AW. A hybrid zinc-calcium-silicate polyalkenoate bone cement. Biomaterials. 2003;24: 2749–57.
34. De Mayer EAP, Verbeeck RMH, Vercruysse CMJ. Infrared spectroscopic study of acid-degradable glass. J Dent Res. 2002; 81(8):552–5.
35. Tomlinson SK, Ghita OR, Hooper RM, Evans KE. Investigation of the dual setting mechanism of a novel dental cement using infrared spectroscopy. Vib Spectrosc. 2007;45:10–7.
36. Dong J, Ozaki Y, Nakashima K. Infrared Raman and near-infrared spectroscopic evidence for the coexistence of various hydrogen-bond forms in poly(acrylic acid). Macromolecules. 1997;30:1111–7.
37. Young AM, Sherpa A, Pearson G, Schottlander B, Waters DN. Use of Raman spectroscopy in the characterization of the acid-base reaction in glass ionomer cements. Biomaterials. 2000;21: 1971–9.
38. Hill RG, Stamboulis A, Law RV, Clifford A, Towler MR, Crowley C. The influence of strontium substitution in fluorapatite glasses and glass-ceramics. J Non-Cryst Solids. 2004;336(3): 223–9.
39. Matsuya S, Maeda T, Ohta M. IR and NMR analysis of hardening and maturation of glass ionomer cement. J Dent Res. 1996;75: 1920–7.
40. Crisp S, Pringuer MA, Wardleworth D, Wilson AD. Reactions in glass ionomer cements: II. An infrared spectroscopic study. J Dent Res. 1974;53:1414–1419.